AIAA JOURNAL
Vol. 47, No. 12, December 2009

Effects of Turbulent Boundary Layer on Panel Flutter

Atsushi Hashimoto* and Takashi Aoyama†
Japan Aerospace Exploration Agency, Chofu, Tokyo, 182-8522, Japan
and
Yoshiaki Nakamura‡
Nagoya University, Nagoya, Aichi, 464-8603, Japan

DOI: 10.2514/1.35786

Numerical studies were carried out to investigate the effects of turbulent boundary layers on panel flutter at supersonic speeds. In this study, Reynolds-averaged Navier–Stokes equations were solved to take into account the turbulent boundary layer and its viscous effects. First, the fluid–structure coupling code was validated. The computed flutter boundaries agreed well with experimental data. Moreover, the results showed that the viscous effects were important and should be taken into account for flutter computation. Second, the boundary-layer effects were investigated in the Mach number range of 1.0–2.4. We compared the Reynolds-averaged Navier–Stokes computation with the inviscid computation and discussed the differences between them. We found that the boundary layer has not only a stabilizing effect but also a destabilizing effect, depending on the Mach number. The most important finding is that the flutter dynamic pressure slowly increases due to the boundary layer as the Mach number increases. In addition, the design boundary methodology was reviewed in terms of the turbulent boundary-layer effect, which will be helpful for the development of a new boundary-layer correction for the design boundary.

Nomenclature

A, B, C	=	Jacobian of flux vector
a	=	panel length in the streamwise direction
b	=	panel length in the spanwise direction
c	=	sonic speed
D	=	plate stiffness, $E_s h^3/12(1-\nu^2)$
E, F, G	=	inviscid flux
E_s	=	Young modulus
E_v, F_v, G_v	=	viscous flux
f	=	frequency
h	=	panel thickness
J	=	Jacobian of coordinate transformation
M	=	Mach number
p	=	pressure
Q	=	solution vector
Re	=	Reynolds number
U	=	freestream velocity
x, y, z	=	Cartesian coordinate
δ	=	98% thickness of boundary layer
Δt	=	time step
$\Delta\tau$	=	pseudo time step
λ	=	nondimensional dynamic pressure, $\rho_\infty U_\infty^2 a^3/D$
ν	=	Poisson ratio
ξ, η, ζ	=	generalized coordinate
ρ	=	air density

Subscripts

f	=	value at flutter boundary
invis	=	inviscid computation
vis	=	viscous computation
∞	=	value of freestream

Received 21 November 2007; revision received 7 July 2009; accepted for publication 25 August 2009.

*Researcher, Computational Science Research Group, Institute of Aerospace Technology. Member AIAA.
†Section Leader, Computational Science Research Group, Institute of Aerospace Technology. Member AIAA.
‡Professor, Department of Aerospace Engineering. Member AIAA.

I. Introduction

PANEL flutter is well known as flutter of the skin panel of rockets, supersonic transports, and fighters. This phenomenon is a self-excited oscillation of thin panels due to aeroelastic instability at supersonic speed. Much research on panel flutter has been conducted in the past, theoretically and experimentally, and some results are reviewed in [1,2]. Despite the simple geometry of a panel (e.g., a rectangular panel or shell), it is generally hard to obtain quantitative agreement of flutter boundaries between computation and experiment [3], since there are many factors affecting the boundaries, such as the effects of a turbulent boundary layer above the panel, structural damping, static-pressure differential across the panel, cavity resonance, and manufacturing imperfection. Therefore, efforts have been made to reduce these confounding effects and to measure flutter boundaries under ideal conditions. Nevertheless, those effects were not fully eliminated and it is hard to obtain quantitative agreement, especially in low-supersonic regions ($M = 1.0$–1.4). It is therefore necessary to understand these effects.

Fung [4] indicated that, among those effects, the turbulent boundary layer is the main reason why the computation cannot predict flutter boundaries. Next, Muhlstein et al. [5] and Gaspers et al. [6] investigated the effects of the turbulent boundary layer in low-supersonic regions, using a test fixture that can control the thickness of the boundary layer above a panel. These experiments were performed so as to reduce the confounding effects mentioned above. They concluded that the turbulent boundary layer has a large stabilizing effect on flutter at low-supersonic speeds and that the effect is the largest near $M = 1.2$ and decreases rapidly with increasing Mach number up to $M = 1.4$. Therefore, the effect was believed to appear near $M = 1.2$ (low-supersonic region).

Next, Dowell [7,8] computed the flutter boundaries under experimental conditions [5], taking into account the mean flow variation at the boundary layer. He solved linear perturbation equations to obtain pressure on the panel. In addition, he neglected viscosity and employed a one-seventh power low as the mean velocity profile. Although his computation realized a stabilizing effect, there was poor agreement with the experimental data.

Recently, computational fluid dynamics (CFD) has often been employed for fluid–structure coupled analysis. For panel flutter problems, Davis and Bendiksen [9] first analyzed transonic panel flutter and investigated shock-wave motion on panels using CFD. Then Selvam et al. [10] and Gordnier and Visbal [11] investigated limit cycle oscillation above a flutter boundary and the viscous effects on its amplitude and frequency. However, no comparison with

experimental data was made in their research. Moreover, viscous effects on flutter boundaries were not investigated.

In this study, we investigated the effects of a turbulent boundary layer on flutter boundaries by solving Reynolds-averaged Navier–Stokes (RANS) equations. First, computed flutter boundaries were compared with the experimental data measured by Muhlstein et al. [5] at $M = 1.1$–1.4 to validate our fluid–structure coupled analysis code, taking into account the viscous effects. Next, flutter boundaries at higher Mach numbers ($M = 1.1$–2.4) were computed using the code and were compared to those computed by inviscid flow to clarify the effects of the turbulent boundary layer.

II. Computational Method

A. Aerodynamic Solver

The governing aerodynamic equations are Euler or RANS equations written in generalized coordinates. These equations are solved using the perfect gas relationship. In addition, the molecular viscous coefficient is computed by Sutherland's law and the Prandtl number is assumed to be constant.

In most panel flutter problems, the nondimensional flutter frequency ($St_f = f_f a/U_f$) is much less than 1; they are 0.04–0.08 for $M = 1.1$–1.4 in this problem. In addition, a very thin grid must be used to resolve the viscous sublayer. Therefore, an implicit time integration method should be employed to obtain a solution in practical time. In this study, lower/upper symmetric Gauss–Seidel involving the dual-time-stepping method was employed for time integration. The numerical algorithm is written in delta form as

$$\begin{aligned}&\left(\frac{1}{J}\left(\frac{3}{2\Delta t}+\frac{1}{\Delta\tau}\right)+\frac{\partial}{\partial\xi}A+\frac{\partial}{\partial\eta}B+\frac{\partial}{\partial\zeta}C\right)\Delta Q^m\\&\quad=-\left[\frac{\partial}{\partial\xi}\left(E-\frac{1}{Re}E_v\right)+\frac{\partial}{\partial\eta}\left(F-\frac{1}{Re}F_v\right)\right.\\&\quad\left.+\frac{\partial}{\partial\zeta}\left(G-\frac{1}{Re}G_v\right)\right]^m-\frac{1}{J}\frac{3Q^m-4Q^n+Q^{n-1}}{2\Delta t}\\&\quad+Q^m\left[\left(\frac{\xi_t}{J}\right)_\xi+\left(\frac{\eta_t}{J}\right)_\eta+\left(\frac{\zeta_t}{J}\right)_\zeta\right]^m\Delta Q^m=Q^{m+1}-Q^m\end{aligned}\quad(1)$$

where n is a physical time step number and m is a subiteration number. When a sufficient subiteration number is used, second-order time accuracy is achieved in this formulation. The last term at the right-hand side computes a Jacobian time derivative using the geometric conservation law.

Inviscid fluxes on the right-hand side are computed by Roe's approximate Riemann solver with third-order MUSCL interpolation, whereas viscous fluxes are computed by a second-order central difference. Regarding the turbulence model, we mainly employed the Baldwin–Lomax (BL) model [12], since the nondimensional flutter frequency St_f is relatively low. We also employed the Spalart–Allmaras (SA) model [13] to see the effects of turbulence models. The BL model is a simple zero-equation model, whereas the SA model is a one-equation model including a convection term.

B. Structure Solver

The turbulent boundary layer forms a moderate pressure gradient in the streamwise direction above the panel, and the cavity pressure (the pressure under the panel) is assumed to be constant in this study. Therefore, the panel may deflect due to the static-pressure differential across the panel, and its deflection can become large and nonlinear, depending on the pressure differential. To avoid an unphysical large deflection, we employed the von Kármán plate equations [14] that are nonlinear large-deformation plate equations considering in-plane stresses. We solved the equations by a finite difference method (FDM) [14]. A second-order central difference was employed for space derivatives, and Newmark's β method was employed for time integration.

C. Fluid–Structure Coupling method

To solve aerodynamics and structure dynamics simultaneously, a strong coupling method was used in which data is exchanged between the aerodynamic solver and structure solver in every step of the subiteration. This method can reduce the time lag between the two solvers [10].

Nonslip boundary conditions are implemented by setting the flow velocity on the panel surface equal to that of the panel surface. The deformation velocity and acceleration of the panel are transferred from the structure solver to the aerodynamic solver as boundary conditions, where acceleration is considered by setting the pressure gradient on the surface using the following equation:

$$\frac{\partial p}{\partial n}=-\rho\mathbf{a}\cdot\mathbf{n}\quad(2)$$

where p is pressure, ρ is density, $\mathbf{a}$ is the acceleration vector, and $\mathbf{n}$ is the unit vector normal to the surface. Additionally, we neglect the normal viscous stress in the equation because the Reynolds number is high. In this study, we employ the same size grid on the panel both for aerodynamic and structural computations to transfer the data easily between the two solvers.

The grid moves with the panel deflection. It is redistributed smoothly normal to the panel surface using algebraic equations [15], whereas the grid on the far-field boundary is kept fixed to simplify the treatment of far-field boundary conditions.

III. Computational Conditions

In this study, we employ the panel configuration and flow conditions of Muhlstein et al.'s [5] experiment. The panel configuration is shown in Fig. 1. The panel length/width ratio a/b is 0.5 and all sides are clamped. In addition, the boundary-layer thickness above the panel, δ, is defined as the 98% thickness at the middle of the panel, as shown in Fig. 1. We mainly use the 10% panel length thickness, $\delta/a = 0.1$.

The computational domain employed in this study is shown in Fig. 2, which also shows the domain size. The upper boundary is high enough to avoid reflection of the shock wave from the leading edge of the wall. The adiabatic wall conditions are used for the lower boundary, and the first-order extrapolation is used for the outflow boundary. Additionally, the freestream conditions are imposed for the other boundaries. Moreover, the distance between the inflow boundary and the panel front edge, Lx, is adjusted to realize the desired boundary-layer thickness. In addition, the cavity pressure is assumed to be constant. In this study, we took the average pressure on the upper surface of the panel as the cavity pressure. In fact, the cavity pressure in the experiment was also controlled to minimize the differential pressure across the panel [5].

As for the grid numbers, 90, 59, and 95 points are used in the streamwise, spanwise, and normal directions, respectively, of which

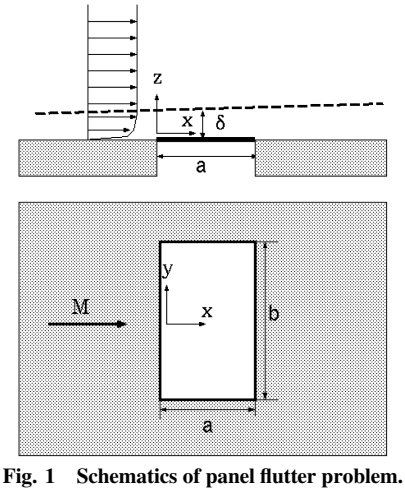

Fig. 1 Schematics of panel flutter problem.

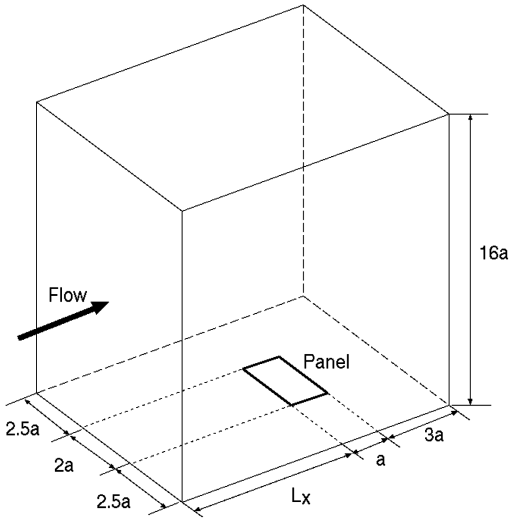

Fig. 2 Computational domain.

20 points in the streamwise direction and 40 points in the spanwise direction are distributed on the panel.

An initial velocity is imposed on the panel at the beginning of the coupled simulation using the following distribution function:

$$v(x, y) = v_{\text{ini}} \sin^2(\pi x/a) \sin^2(\pi y/b) \tag{3}$$

where x is $0 \le x \le a$ and y is $0 \le y \le b$. The coefficient v_{ini} is $0.01c$ (c is sonic speed). For the viscous cases, the flowfield is computed to obtain the converged solution of the turbulent boundary layer in advance. Then the solution is used as the initial condition of the coupled simulation, and the flutter boundaries are determined by computing several cases with a changing Young modulus at a constant Mach number and mass ratio. The computed flutter boundaries are compared with experimental data using the nondimensional dynamic pressure λ. Additionally, since the initial response is affected by the initial velocity and its distribution, the simulation is continued until the oscillation mode is converged.

IV. Results

A. Dependency on Grid and Time Step

In the previous study [16], we analyzed panel flutter in a laminar and turbulent boundary layer on the panel. The results show that the flutter boundaries are largely affected by the boundary layer, and there is a large difference in the flutter boundaries between the laminar and turbulent boundary layers. The laminar boundary layer has a larger stabilizing effect than the turbulent boundary layer at the same Reynolds number, $Re = 10^5$, though the laminar boundary layer is thinner than the turbulent boundary layer. Thus, both the boundary-layer thickness and the velocity profile are important to determine the flutter boundaries. Therefore, the velocity profile of the boundary layer must be computed accurately. Moreover, the time step is also important for fluid–structure coupled problems, as mentioned in [10]. To compute accurate flutter boundaries of the panel in the turbulent boundary layer, dependency on grid resolution and time step is examined.

We examine the dependency for the cases in which the minimum grid sizes in the normal direction to the panel, Δz, are 5×10^{-5}, 2×10^{-5}, 1×10^{-5}, and 5×10^{-6} and the time steps Δt are 1.25×10^{-3}, 2.5×10^{-3}, 5.0×10^{-3}, and 1.0×10^{-2}, where z and t are nondimensionalized by a and $a \times c$, respectively. All cases are computed under the conditions of $M = 1.2$ and $\delta/a = 0.1$. In addition, the subiteration is used three times for each physical time step in all cases. The computed flutter boundaries are shown in Figs. 3 and 4. The flutter boundary is largely affected by the grid resolution and time step. As the time step decreases, the flutter dynamic pressure decreases. Conversely, as the grid size decreases, the flutter dynamic pressure increases. The limiting values are estimated by Richardson

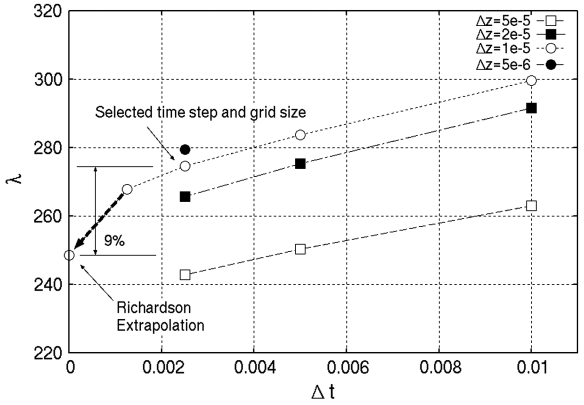

Fig. 3 Effect of time step Δt on flutter boundary.

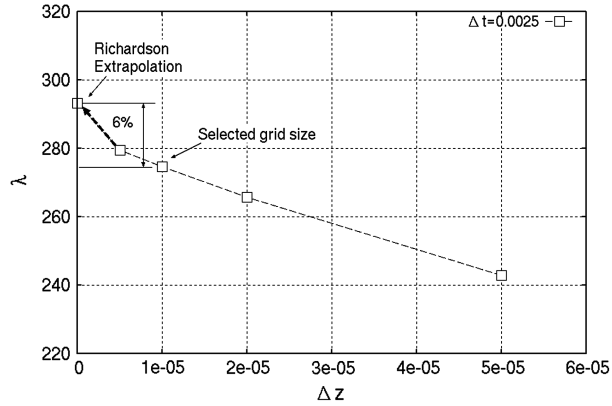

Fig. 4 Effect of grid size Δz on flutter boundary.

extrapolation [17]. Although the smallest time step and grid size are favorable, we selected 2.0×10^{-5} and 2.5×10^{-3} for Δz and Δt, respectively, to keep the computational time needed within reason. The estimated errors are 6–9% in nondimensional dynamic pressure (Figs. 3 and 4), which is smaller than the variation due to the boundary layer, as described later. In addition, when the grid size is evaluated by y^+ (wall distance measured in viscous length scale), y^+ is 0.92 at the middle of the panel for Δz of 2.0×10^{-5} and is sufficiently small. When the time step is used, approximately 5300 steps are included in a period of oscillation at $M = 1.2$ and $\delta/a = 0.1$. These selected grid size and time step are used for the following computation.

B. Structure Model

Table 1 shows the natural frequencies of the first to fifth modes of the panel computed by the FDM, and the experimental data [6] is also shown for comparison. The corresponding mode shapes are illustrated in Fig. 5. Although errors of approximately 10% were observed in the third and fourth modes, the natural frequencies show reasonable agreement as a whole. The errors of the higher-mode frequencies seem to be due to the different boundary conditions between computation and experiment. In fact, the edge condition of the panel in the experiment is not the ideal clamp condition, as mentioned in [6]. However, in this problem, the panel mainly oscillates

Table 1 Structure oscillation frequency

	Mode				
	1	2	3	4	5
FDM, Hz	108.1	138.2	191.7	267.9	278.4
Exp, Hz	110.0	143.0	212.0	298.0	287.0
Error, %	1.7	3.4	9.6	10.1	3.0

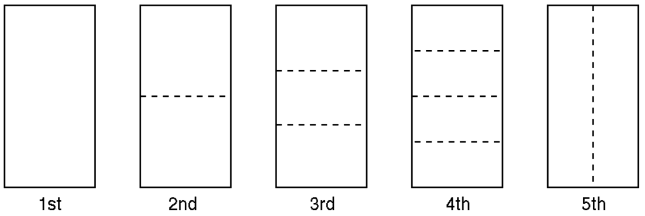

Fig. 5 Node line of natural mode.

with the first mode for the lower Mach numbers ($1 < M \leq 1.4$) and with the first and fifth modes for higher Mach numbers ($M > 1.4$). Therefore, the effect caused by the errors is thought to be small.

C. Euler Computation

Euler computation was carried out for Mach 1.1–1.4. The flutter boundaries determined by Euler computation are compared with Dowell's computation [7] and the experimental data [5] (Fig. 6). Dowell [7] computed them using an inviscid small-perturbation theory, whereas the experimental data are extrapolated values from the flutter boundaries measured at different boundary-layer thicknesses. The flutter dynamic pressure obtained by the present method is lower for Mach 1.1–1.2 and rapidly increases with the Mach number. This computational result agrees well with Dowell's computation, and agreement with experimental data is good except for $M = 1.4$. The difference at $M = 1.4$ seems to be due to the different panel boundary conditions mentioned in the previous section, since the component of the third natural mode is larger only at $M = 1.4$.

D. RANS computation

Next, RANS computation was carried out at $M = 1.2$ considering the turbulent boundary layer. Here, we employed the BL model for the turbulence model. Flutter dynamic pressures are computed for the boundary-layer thicknesses in the range of $\delta/a = 0.03$–0.11. Figure 7 compares the computation and experiment [5] flutter boundaries. As the thickness of the boundary layer increases, the flutter dynamic pressure increases. The obtained results quantitatively agree well with the experimental data; the boundary layer has a stabilizing effect (i.e., increased flutter dynamic pressure) on flutter at $M = 1.2$. In addition, the flutter boundary obtained by inviscid (Euler) computation is also shown at $\delta/a = 0$ in Fig. 7. The inviscid flutter boundary is near the asymptotic value at $\delta/a = 0$ of the flutter boundaries for $\delta/a = 0.03$–0.11.

Figure 8 shows a snapshot of a fluttering panel, illustrating the deflected panel and pressure on the panel surface. The deflection is amplified in the visualization process so that the oscillation mode can be identified. The computational conditions are $M = 1.2, \delta/a = 0.1$, and $\lambda = 280$. As shown in Fig. 8, the panel oscillates at almost the first mode at this Mach number. In addition, the pressure on the panel

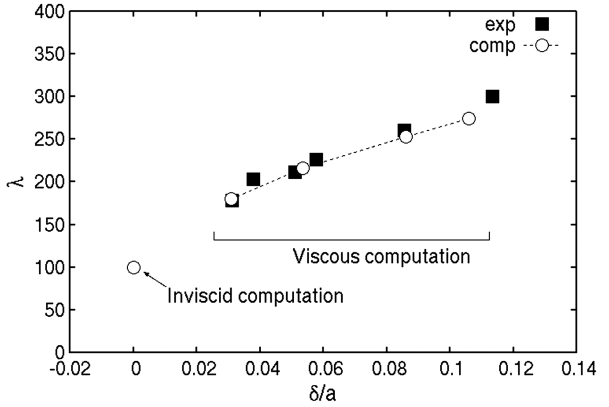

Fig. 7 Flutter boundaries vs boundary-layer thickness ($M = 1.2$).

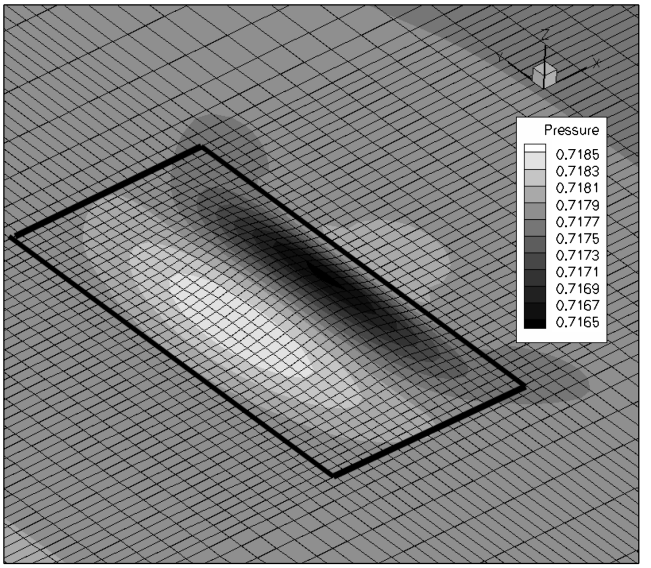

Fig. 8 Fluttering panel and surface pressure.

changes according to the defection. For example, at the moment shown in the figure, the surface pressure is high on the front side due to the compression waves and low in the back side due to the expansion waves.

RANS computation was carried out at Mach 1.1–1.4 using BL and SA models. The results are shown in Fig. 9, in which the computed boundaries are compared with Dowell's computation [7] and the experimental data [5]. Dowell [7] computed them using an inviscid small-perturbation theory based on a mean flow of turbulent

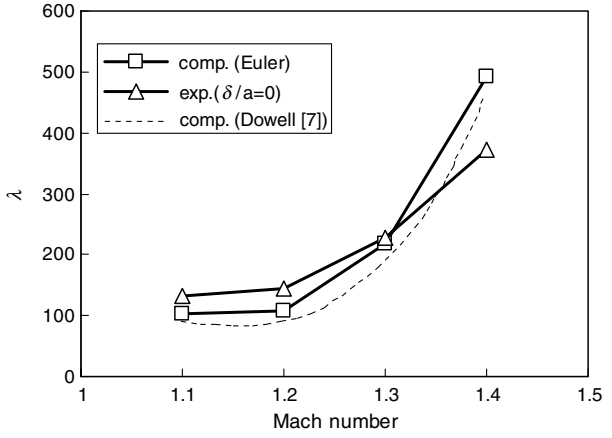

Fig. 6 Flutter boundary (inviscid case).

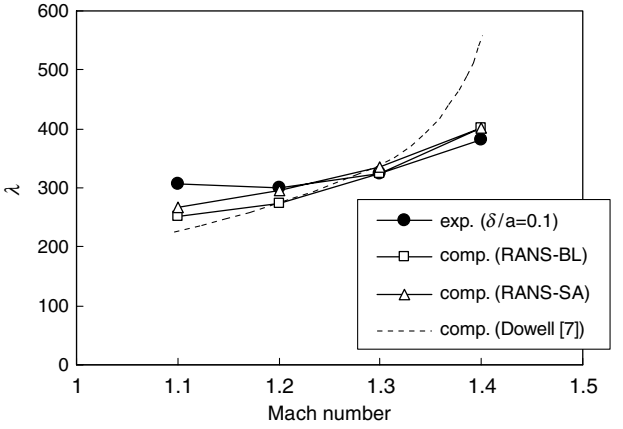

Fig. 9 Flutter boundary (viscous case).

boundary layer, but he did not include the viscous effect. As shown in Fig. 9, the two computational results using BL and SA models agree well with the experimental data and show better agreement than Dowell's computation at Mach 1.4. This difference comes from the viscous effect that is neglected in Dowell's computation. In fact, Dowell's computation shows a similar feature to the inviscid computation, in which the flutter dynamic pressure increases rapidly with the Mach number (Fig. 6). In the present computation, however, the flutter dynamic pressure increases slowly. As mentioned above, the present computational code accurately predicts the flutter boundaries. Moreover, the viscous effect is significantly important and should be taken into account in the analysis: otherwise, the flutter boundaries cannot be predicted accurately. In addition, the panel flutter problem employed in this study is recommended as a benchmark problem to validate a fluid–structure coupled code treating a turbulent flow, since the turbulent boundary-layer effect on flutter can be examined directly and clearly.

The two models, BL and SA, predict the flutter boundaries well and the difference between the two models is small, as shown in Fig. 9, though the flutter boundaries of the SA model are slightly higher than those of the BL model. The Baldwin–Lomax model is a quasi-steady approximation of the turbulent boundary layer. The results show that the modeling is appropriate in this problem, probably because the nondimensional flutter frequency St_f is low. Therefore, we use the simple BL model hereafter.

E. Effect of Turbulent Boundary Layer

Since the fluid–structure coupled code is well validated, the effects of the boundary layer were investigated further over a wide range of Mach numbers. We conducted the RANS computation using the BL model at $\delta/a = 0.1$ and $M = 1.1$–2.4. Since there is no available experimental data for $M \geq 1.5$, the mass ratio for Mach number 1.4 was used for $M \geq 1.5$ as well. We also conducted inviscid computations for purposes of comparison. The computed flutter boundaries are shown in Fig. 10. In the low-supersonic region, $M = 1.1$–1.3, the flutter dynamic pressures at $\delta/a = 0.1$ are much higher than those of inviscid case. Thus, flutter is stabilized by the boundary layer in this region. Then the flutter dynamic pressure of the inviscid case increases rapidly near $M = 1.4$, a feature similar to Dowell's computation [1]. On the other hand, the flutter dynamic pressure at $\delta/a = 0.1$ increases more slowly than that of the inviscid case. This slow increase causes inversion of the flutter boundary in the region $M = 1.4$–1.8, where flutter is destabilized by the boundary layer. Further, the flutter dynamic pressure at $\delta/a = 0.1$ becomes higher than that of the inviscid case for $M \geq 2.0$.

Figure 11 shows the difference in flutter boundaries between the viscous (RANS) and inviscid (Euler) computations, and this difference is evaluated in the following equation:

$$\text{diff} = \frac{\lambda_{\text{vis}} - \lambda_{\text{invis}}}{\lambda_{\text{invis}}} \times 100\,\%$$

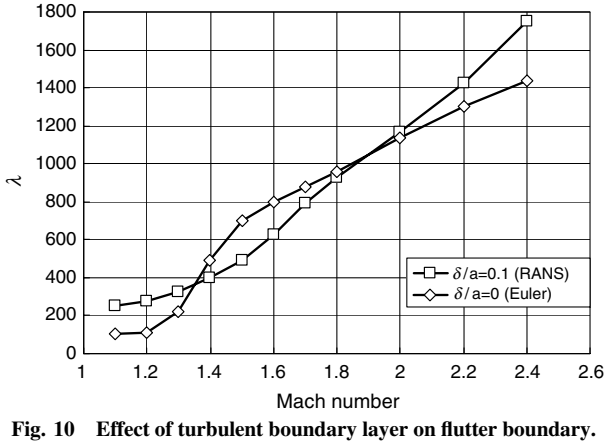

Fig. 10 Effect of turbulent boundary layer on flutter boundary.

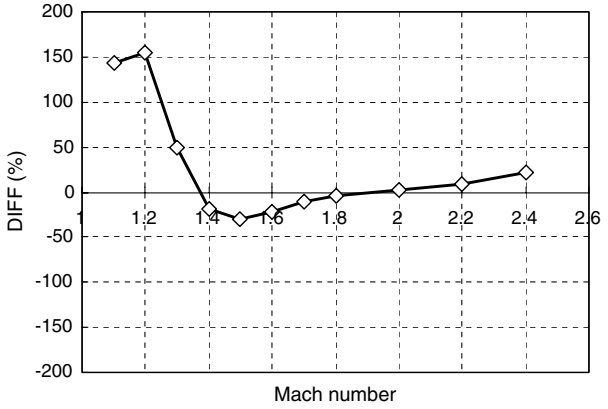

Fig. 11 Difference between inviscid and viscous computations.

From the figure, the difference appears mainly in the low-supersonic region. At $M = 1.4$–1.6, the difference is approximately 30%. Even recently, quasi-steady aerodynamic theory has been commonly used, especially for higher Mach numbers (e.g., $M > 1.5$). Since the flutter boundaries computed by Euler equations are almost the same as those computed by the quasi-steady aerodynamic theory for $M > 1.5$ [9], this difference is thought to be the difference between the viscous computation and the quasi-steady aerodynamic theories.

The effects of a turbulent boundary layer on panel flutter were discussed by Muhlstein et al. [5], Gaspers et al. [6], and Dowell [7,8]. Their discussions are limited to the stabilizing effect of flutter in the low-supersonic region ($1.1 \leq M \leq 1.3$), since the effect was thought at that time to be the largest in this region. In fact, the effect is large in this region, as shown in Fig. 11. However, it is necessary to consider a wide range of Mach numbers in order to understand the effects of the boundary layer. As shown in Fig. 10, the boundary layer not only has a stabilizing effect but also a destabilizing effect. The most important finding here is that the flutter dynamic pressure slowly increases due to the boundary layer at $M = 1.4$–1.6. One possible reason for this slow increase could be an effect secondary to the local Mach number reduction. Because the flow near the panel becomes slow due to the boundary layer, the characteristics at the lower Mach numbers ($1 < M \leq 1.4$) continue even at higher Mach numbers ($M \geq 1.5$).

F. Comparison with Design Boundary

In the design process of a skin panel, semi-empirical methodologies [18,19] are commonly used to prevent panel flutter. Although the methodologies were developed in the 1960s and 1970s, they are still used for designs even these days, such as the Quiet Spike panel design [20]. Here, we compare the methodology [19] with the present computation.

The method developed by Laurenson and McPherson [19] is very simple for an isotropic panel clamped at all sides, such as the panel used in this study. The nondimensional dynamic pressure is expressed as a function of Mach number M and the length/width ratio a/b:

$$\lambda = \frac{2f(M)}{\text{FP}(a/b)} \tag{4}$$

where $f(M)$ is the Mach number correction factor and $\text{FP}(a/b)$ is the flutter parameter determined by the length/width ratio. In addition, two kinds of Mach number correction factors are available, depending on the Mach number. For $M > 2.0$, the Mach number correction factor $f_1(M) = \sqrt{M^2 - 1}$ was used. In fact, the use of this factor yields flutter boundaries that show generally good agreement with those given by theories (e.g., the quasi-steady aerodynamic theory) for the Mach numbers [19]. On the other hand, the Mach number correction factor f_2, shown in Fig. 12, was used for $1.0 < M \leq 2.0$, which is a curve-fitting of the low-supersonic experimental data measured by Kappus et al. [21]. In addition, the correction factor f_2 has a dependency on the length/width ratio a/b, and only the correction factor for $a/b = 0.5$ is shown in Fig. 12. The

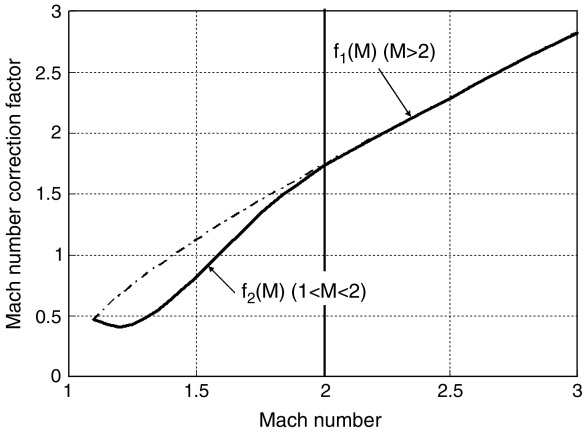

Fig. 12 Mach number correction factor.

FP corresponding to the length/width ratio is determined from the design boundary envelope shown in Fig. 3 of [19]. In this problem, the flutter parameter FP is 3×10^{-3} for the length/width ratio of 0.5.

The design flutter boundaries using $f_1(M)$ and $f_2(M)$ are shown in Fig. 13 and are compared with the present computations. For $M < 2.0$, the design boundaries using $f_2(M)$ agree well with the present RANS computation, despite the simple calculation using only the length/width ratio and Mach number. In fact, the experimental data used for the correction factor $f_2(M)$ was measured at the NASA Ames Research Center 2×2 foot transonic wind tunnel. It is the same as the wind tunnel used in Muhlstein et al's [5] experiment, the data from which are used for the validation of this study. Therefore, the boundary-layer thicknesses are almost the same, and this is a reason for the observed good agreement. Moreover, this result shows that the Mach number correction factor $f_2(M)$ includes not only the low-supersonic Mach number effect but also the boundary-layer effects. We have to note that the design boundary does not consider the boundary-layer thickness δ/a. Therefore, the flutter boundary may change with the thickness, and a RANS computation is required to determine accurate flutter boundaries.

For $M > 2.0$, the design boundaries agree well with the Euler computation. Although the background theory used for the methodology is not explained in detail in [19], the design boundaries are almost the same as those computed by the inviscid flow for $M > 2.0$. Thus, the correction factor $f_1(M)$ does not include the effect of the boundary layer. The Mach number correction factors f_1 and f_2 are inconsistent. Factor f_1 does not include the boundary-layer effects, whereas factor f_2 does include them. In addition, the flutter boundaries obtained by the RANS computation are a little higher than those obtained by the Euler computation for $M > 2.0$ (Fig. 13), though the difference is relatively small in this region compared to the low-supersonic region (Fig. 11). As mentioned above, the design boundary has been reviewed in terms of the turbulent boundary-layer effect in this study, which will be helpful for the development of a new boundary-layer correction for the design boundary.

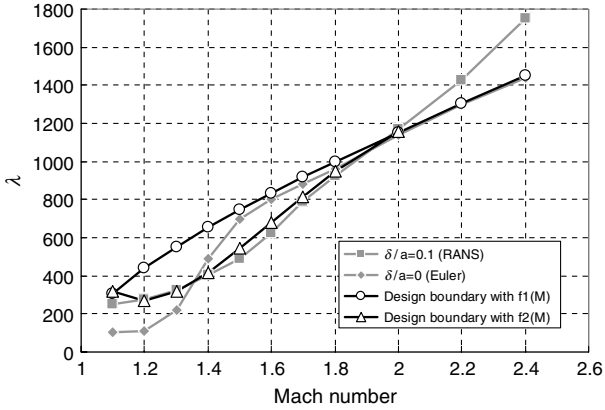

Fig. 13 Comparison between the design boundary and the computed boundary by the present method.

V. Conclusions

We numerically investigated the effects of turbulent boundary layers on panel flutter. In this study, Reynolds-averaged Navier–Stokes (RANS) equations were solved using computational fluid dynamics (CFD) to take the turbulent boundary layer into account, and von Kármán plate equations were solved for the panel. First, the fluid–structure coupling code was validated. The grid resolution and time step were carefully selected before the computation. As a result, the flutter boundaries computed by RANS equations quantitatively agree well with the experimental data. Moreover, the comparison between the present and Dowell's [7] computations showed that the viscous effect is significantly important and should be taken into account. In this study, the flutter boundaries with Baldwin–Lomax and Spalart–Allmaras models are compared and the difference between them is found to be small. In addition, the panel flutter problem used in this study is recommended as a benchmark problem to validate a fluid–structure coupled code treating a turbulent flow, since the turbulent boundary-layer effect on flutter can be examined directly and clearly.

Then the flutter boundaries in the range $M = 1.1$–2.4 were computed using the code and compared with those computed by inviscid flow in order to clarify the effects of a turbulent boundary layer. It was found that the boundary layer not only has a stabilizing effect but also a destabilizing effect, depending on the Mach number. The most important finding is that the flutter dynamic pressure increases slowly due to the boundary layer as the Mach number increases in the range $M = 1.2$–1.5.

The design boundaries proposed by Laurenson and McPherson [19] agree with the present RANS computation in the low-supersonic region, whereas they agree with the Euler computation for $M > 2.0$. It was found that the Mach number correction factor of the design boundary for the lower Mach numbers ($1 < M \leq 2$) includes the turbulent boundary-layer effects. In addition, the design boundary does not consider the parameter of boundary-layer thickness δ/a, and therefore the boundary may change with the thickness. Thus, a new correction is needed for the boundary layer. In this paper, the design boundary was reviewed in terms of the turbulent boundary-layer effect, which will be helpful for the development of the new boundary-layer correction for the design boundary.

References

[1] Dowell, E. H., "A Review of the Aeroelastic Stability of Plate and Shells," *AIAA Journal*, Vol. 8, No. 3, 1970, pp. 385–399. doi:10.2514/3.5680

[2] Mei, C., Abdel-Motagaly, K., and Chen, R., "Review of Nonlinear Panel Flutter at Supersonic and Hypersonic Speeds," *Applied Mechanics Reviews*, Vol. 52, No. 10, 1999, pp. 321–332. doi:10.1115/1.3098919

[3] Dowell, E. H., "Theoretical and Experimental Panel Flutter Studies in the Mach Number Range 1.0 to 5.0," *AIAA Journal*, Vol. 3, No. 12, 1965, pp. 2292–2304. doi:10.2514/3.3359

[4] Fung, Y. C., "Some Recent Contribution to Panel Flutter Research," *AIAA Journal*, Vol. 1, No. 4, 1963, pp. 898–909. doi:10.2514/3.1661

[5] Muhlstein, L., Gaspers, P. A., and Riddle, D. W., "An Experimental Study of the Influence of the Turbulent Boundary Layer on Panel Flutter," NASA TN D-4486, 1968.

[6] Gaspers, P. A., Muhlstein, L., and Petroff, D. N., "Further Experimental Results on the Influence of The Turbulent Boundary Layer on Panel Flutter," NASA TN D-5798, 1970.

[7] Dowell, E. H., "Generalized Aerodynamic Forces on a Flexible Plate Undergoing Transient Motion in a Shear Flow with an Application to Panel Flutter," *AIAA Journal*, Vol. 9, No. 5, 1971, pp. 834–841. doi:10.2514/3.6283

[8] Dowell, E. H., "Aerodynamic Boundary Layer Effects on Flutter and Damping of Plates," *Journal of Aircraft*, Vol. 10, No. 12, 1973, pp. 734–738.

doi:10.2514/3.60298
[9] Davis, G. A., and Bendiksen, O. O., "Transonic Panel Flutter," AIAA Paper 93-1476, 1993.
[10] Selvam, R. P., Visbal, M. R., and Morton, S. A., "Computation of Nonlinear Viscous Panel Flutter Using a Fully-Implicit Aeroelastic Solver," AIAA Paper 98-1844, 1998.
[11] Gordnier, R. E., and Visbal, M. R., "Development of a Three-Dimensional Viscous Aeroelastic Solver for Nonlinear Panel Flutter," *Journal of Fluids and Structures*, Vol. 16, No. 4, 2002, pp. 497–527.
doi:10.1006/jfls.2000.0434
[12] Baldwin, B. S., and Lomax, H., "Thin Layer Approximation and Algebraic Model for Separated Turbulent Flows," AIAA Paper 78-257, 1978.
[13] Spalart, P. R., and Allmaras, S. R., "A One-Equation Turbulence Model for Aerodynamic Flows," AIAA Paper 92-0439, 1992.
[14] Brown, J. C., and Harvey, J. M., "Large Deflection of Rectangular Plates Subjected to Uniform Lateral Pressure and Compressive Edge Loading," *Journal of Mechanical Engineering Science*, Vol. 11, No. 3, 1969, pp. 305–317.
doi:10.1243/JMES_JOUR_1969_011_038_02
[15] Gordnier, R. E., and Visbal, M. R., "Development of a Three-Dimensional Viscous Aeroelastic Solver for Nonlinear Panel Flutter," AIAA Paper 2000-2337, 2000.
[16] Hashimoto, A., Yagi, N., and Nakamura, Y., "Effects of Boundary Layer on Supersonic Panel Flutter," *Journal of the Japan Society for Aeronautical and Space Sciences*, Vol. 55, No. 639, 2007, pp. 159–164.
doi:10.2322/jjsass.55.159 (in Japanese).
[17] Roache, P. J., *Verification and Validation in Computational Science and Engineering*, Hermosa, Socorro, NM, 1998.
[18] Lemley, C. E., "Design Criteria for the Prediction and Prevention of Panel Flutter," Air Force Flight Dynamics Lab., TR-67-140, Wright-Patterson AFB, OH, 1968.
[19] Laurenson, R. M., and McPherson, J. I., "Design Procedures for Flutter-Free Surface Panels," NASA CR-2801, 1977.
[20] Simmons, F., Freund, D., Spivey, N. D., and Schuster, L., "Quiet Spike™: The Design and Validation of an Extendable Nose Boom Prototype," AIAA Paper 2007-1774, 2007.
[21] Kappus, H. P., Lemley, C. E., and Zimmerman, N. H., "An Experimental Investigation of High Amplitude Panel Flutter," NASA CR-1837, 1971.

A. Tumin
Associate Editor